Decay and expansion of the early aftershock activity following the 2011, M_w9.0 Tohoku earthquake

O. Lengliné,[1,2] B. Enescu,[3,4] Z. Peng,[5] and K. Shiomi[3]

[1] The 2011, M_w9.0 Tohoku earthquake was followed by an abundant amount of seismicity providing a unique opportunity to analyze the triggering mechanism of great earthquakes. Although the Tohoku earthquake occurred close to a dense seismic network, many aftershocks that occurred in the first few hours after the mainshock are not recorded in the earthquake catalogs. Here we use a template waveform approach to recover as many as possible missing events in the first 12 hours following the Tohoku mainshock. Our analysis is able to detect about 1.4 times more events than those listed in the High Sensitivity Seismograph (Hi-net) earthquake catalog. Combining our new dataset with earthquakes that occurred at latter times, we are able to observe a continuous decay of the aftershock rate and along strike expansion of aftershock area. We relate the latter observation to the occurrence of post-seismic slip over the deep interface. **Citation:** Lengliné, O., B. Enescu, Z. Peng, and K. Shiomi (2012), Decay and expansion of the early aftershock activity following the 2011, M_w9.0 Tohoku earthquake, *Geophys. Res. Lett.*, *39*, L18309, doi:10.1029/2012GL052797.

1. Introduction

[2] Early aftershock activity carries useful information regarding the triggering mechanism of earthquakes [e.g., *Helmstetter and Shaw*, 2009]. Accurate detections and characterization of this activity are thus needed to interpret the evolution of aftershock sequences. Quantifying this activity is also important when analyzing earthquake rate changes caused by sudden stress variations [e.g., *Toda et al.*, 2011]. Unfortunately, numerous earthquakes are often missing in earthquake catalogs following large events due to a large number of events occurring in a short time interval and to the coda-noise generated by the large events of the sequence [e.g., *Kilb et al.*, 2007]. To overcome this issue, earthquake detection can be improved using the correlation of the continuous seismic signal with pre-determined template events. The waveform matching technique has been proven successful in detecting low frequency earthquakes (LFE) from tremor signals [e.g., *Shelly et al.*, 2007] and recovering missing earthquakes during aftershock [e.g., *Lengliné and Marsan*, 2009; *Peng and Zhao*, 2009], foreshock [*Bouchon et al.*, 2011; *Kato et al.*, 2012] and remotely triggered earthquake sequences [*Meng et al.*, 2012]. Such a technique is capable of identifying earthquakes even when the signal to noise ratio at individual stations is relatively low. It also provides the possibility of estimating the position and magnitude of the detected events, based on the location and magnitude of the template signal.

[3] The 2011, M_w9.0 Tohoku megathrust earthquake produced an unprecedented amount of seismic activity providing a unique opportunity to analyze the earthquake triggering caused by such a mega-earthquake. However, because the aforementioned incompleteness of the catalog, especially immediately after the mainshock, the genuine patterns of seismicity changes remain to be revealed.

[4] We use the waveform matching technique to identify aftershocks in the first 12 hours following the 2011 Tohoku earthquake. We show that our method is capable of recovering many missed aftershocks even by the most complete earthquake catalog during this time period (the Hi-net catalog). Magnitude and position of the newly detected events are also estimated. We find an apparent continuous decay of the aftershock rate during the entire time interval investigated in this study. Our results also suggest that the aftershocks, in the down-dip portion of the subduction interface, expanded southward, extending the initial size of the aftershock area.

2. Data

[5] We use continuous seismic recording from 227 stations of the Japanese High Sensitivity Seismograph Network (Hi-net), operated by NIED (Figure 1). All stations are recording at a sampling rate of 100 Hz and for most sites all the 3-component seismograms were available, resulting in 661 continuous records. Most of the continuous waveforms are 12 hours and 10 minutes long and start on March 11, 2011 at 14:45:00 local time, i.e., about 1 minute before the mainshock origin time (14:46:18). Template events are selected as all $m > 3.5$ events of the Hi-net catalogue that occurred in the first 8 days following the mainshock, around the mainshock rupture plane. This selection leaves us with 1401 template events, which are distributed all over the fault plane area (Figure 1). For each template event waveform record, we extract windows around the P- and S-wave arrival times, at all stations and on components where picking times, made by visual inspection by Hi-net operators, are available. The windows are 512 points long (5.12 s) and start 128 points

[1]IPGS, CNRS, Université de Strasbourg, Strasbourg, France.
[2]Seismological Laboratory, California Institute of Technology, Pasadena, California, USA.
[3]Earthquake and Volcano Research Unit, National Research Institute for Earth Science and Disaster Prevention (NIED), Tsukuba, Japan.
[4]Earth Evolution Sciences Department, Faculty of Life and Environmental Sciences, University of Tsukuba, Tsukuba, Japan.
[5]School of Earth and Atmospheric Sciences, Georgia Institute of Technology, Atlanta, Georgia, USA.

Corresponding author: O. Lengliné, IPGS, CNRS, Université de Strasbourg, 5 rue René Descartes, F-67084 Strasbourg CEDEX, France. (lengline@unistra.fr)
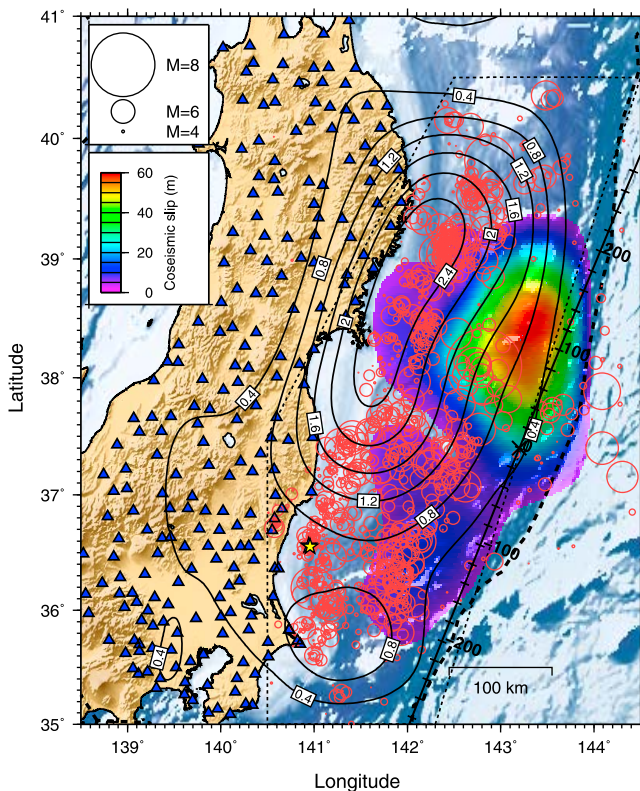
Figure 1. Map of the studied area off the coast of Honshu, Japan (boundaries for selecting detections are shown by black dashed lines). Blue triangles are Hi-net stations for which we have at least one record. Circles represent the template events used in this study and circles size is related to event magnitude. Both the coseismic (color-coded) and postseismic slip (black contours) are updates of those obtained by *Ozawa et al.* [2011]. The coseismic model is estimated from the onshore GPS data and seafloor GPS/acoustic observations (Geospatial Information Authority of Japan, Onshore and offshore crustal deformation and the coseismic slip distribution of the 2011 Tohoku-Oki earthquake, 2011, http://www.gsi.go.jp/cais/topic110520-index.html) and the afterslip distribution is based on the GPS data until October 30, 2011 (Geospatial Information Authority of Japan, Postseismic deformation and the afterslip distribution estimated from GEONET data, 2011, http://www.gsi.go.jp/cais/topic110314-index.html). The yellow and blue star (almost overlapping in the figure) represent the locations of the template and detected earthquake, respectively, shown as example in Figure 2. The dark line marks the strike of the subduction trench where earthquakes are projected in Figure 4, the cross marks the origin of this projection; the distance along strike is labeled.

before the arrival times. Records are extracted on the vertical component for the P-wave window and on the two horizontal components for the S-wave windows. The mean number of records per template event is 101.

3. Detection

3.1. Computing Coherence

[6] The event detection is performed in the frequency domain by computing the mean coherence between the shifted template waveform and the continuous waveform record in the frequency range [1–6] Hz (see Text S1 in the auxiliary material).[1] For each template event and recording station we obtain a continuous coherence signal that covers the full 12 hours and 10 minutes time interval. The coherence signals are shifted by the corresponding P-wave or S-wave travel times from the template event to the recording station, followed by the stacking of all the coherence signals corresponding to a template event. We finally obtain a mean coherence, $R(t)$, by taking an average over the 24 highest coherence values obtained either from S- or P-wave windows at each time step. If an event has less than 24 records, it is not processed.

3.2. Selection of Possible Detections

[7] Out of the 1401 template events, 1344 have at least 24 records and were assigned a coherence function $R(t)$. For each of theses events, we assign a detection when $R(t)$ exceeded a certain threshold, S. As employed in previous studies [e.g., *Peng and Zhao*, 2009], we define this threshold from the distribution of the coherence values. We set, S as $\mu_R + 5\sigma_R$, where μ_R and σ_R are the mean and standard deviation of $R(t)$ (Figure 2). We finally filter out duplicate detections, i.e., detections obtained from different template events that correspond to the same detected event (see methods in Text S1). We get 881 new events for the first 12 hours after the mainshock. This set complements the 629 events already present in the Hi-net catalog that occurred in the first 12 hours (including the template events) and leads to an overall number of 1510 earthquakes. For each detected event we assign the time for which the value of $R(t)$ is the highest as the origin time and assume its location to be the same as that of the corresponding template event.

[8] As a test of our detection procedure, we consider the template event shown in Figure 2. We are able to detect a close aftershock, included in the catalog, which occurred 16 minutes after the template event. The epicentral distance between these two events is less than 2 km and they have similar magnitude (5.3 and 5.1). Figure 2 shows that at almost all stations, a coherence higher than the background value emerges at the time of the wave arrival of the second event. At some stations far from the template event, we can still observe an increase of coherence whereas no picks were made for the second event. This suggests a better performance of the correlation technique compared to manual picking for identifying phase arrival of closely located events, particularly when the signal to noise ratio is small.

3.3. Magnitude

[9] We first derive a scaling relation between the magnitude difference for pairs of template events and their waveform amplitude ratio (see methods in Text S1). Then we apply this relation to our newly detected events by comparing the waveform amplitudes of the detected event with those of the corresponding template event at the same recording stations.

[10] Although our waveform-based detections significantly improve the completeness of the aftershock dataset, our results may still be affected by some transient changes of the magnitude of completeness. To correct for such
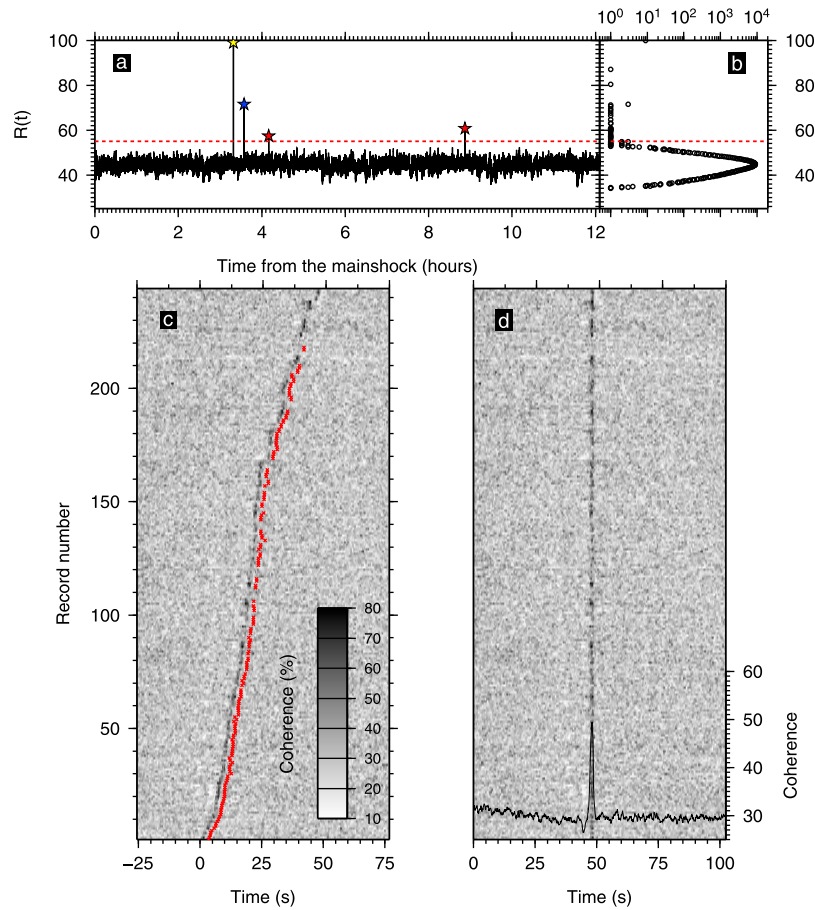

Figure 2. (a) Evolution of the mean coherence, $R(t)$, with time for one template event. We observe the emergence of one peak up to 100% which corresponds to the detection of the current template event itself (yellow star). The blue and red stars show detections associated with this template event. (b) Distribution of the values of $R(t)$. The dashed red line marks the threshold S. (c) Coherence as a function of time for all available records calculated around the pick occurring 16 minutes after the template event (shown by a blue star in Figure 2a). Records are sorted by their arrival times. Red dots correspond to the actual arrival times of the detected event. These arrival times have been shifted to better visualize the coherence value. (d) Same as Figure 2c but time vectors associated to each individual record have been shifted according to the travel times of the template event. The black line is the mean of the coherence signal at all sites along time.

variations, when analyzing the earthquake rate, we follow the method of *Peng et al.* [2007]. We first estimate the b value of the frequency-magnitude distribution for the whole dataset. We find $b = 0.7$, consistent with previous studies in the same area [*Hirose et al.*, 2011; *Kosuga and Watanabe*, 2011; *Marsan and Enescu*, 2012]. Next we compute an estimate of the completeness magnitude as a function of time and use this estimate to compute the expected number of missing events. We finally use these values to compute a corrected earthquake rate.

4. Results

[11] The corrected earthquake rate following the mainshock shows an apparent power-law decay with time during the entire 12 hours interval investigated in this study (Figure 3). We are not able to obtain a reliable estimate of the earthquake rate in the first ∼8 minutes following the mainshock. This is certainly due to a low resolution of our method to detect new events during this time period as the mainshock waveform is still dominating the signal (the

earthquake rupture duration is estimated to be on the order of 4 minutes [*Kiser and Ishii*, 2012]). The power-law exponent, p, of the aftershock decay rate is $p = 0.98 \pm 0.07$ during the first 12 hours. We check that this p-value is not affected by insufficient removal of duplicate events (Figures S1 and S2). We also checked that we obtain the same p-values for threshold magnitudes $m = 4.0$ to 6.0, demonstrating the robustness of our results (Figure 3c). To investigate the evolution of the earthquake rate at latter times, we include in our dataset events reported in the Japan Meteorological Agency (JMA) catalog. The JMA catalog is more complete than the Hi-net catalog at latter times but contains fewer earthquakes in the first 12 hours. The merged catalog containing all events in the first 12 hours is available as Data Set S1 in the auxiliary material. We follow the same procedure as described above to account for possible changes in the magnitude of completeness in the JMA catalog. The earthquake rate at latter time (more than 3 days after the mainshock) also presents a power-law decay behavior with $p = 1.02 \pm 0.07$, comparable to *Hirose et al.* [2011].
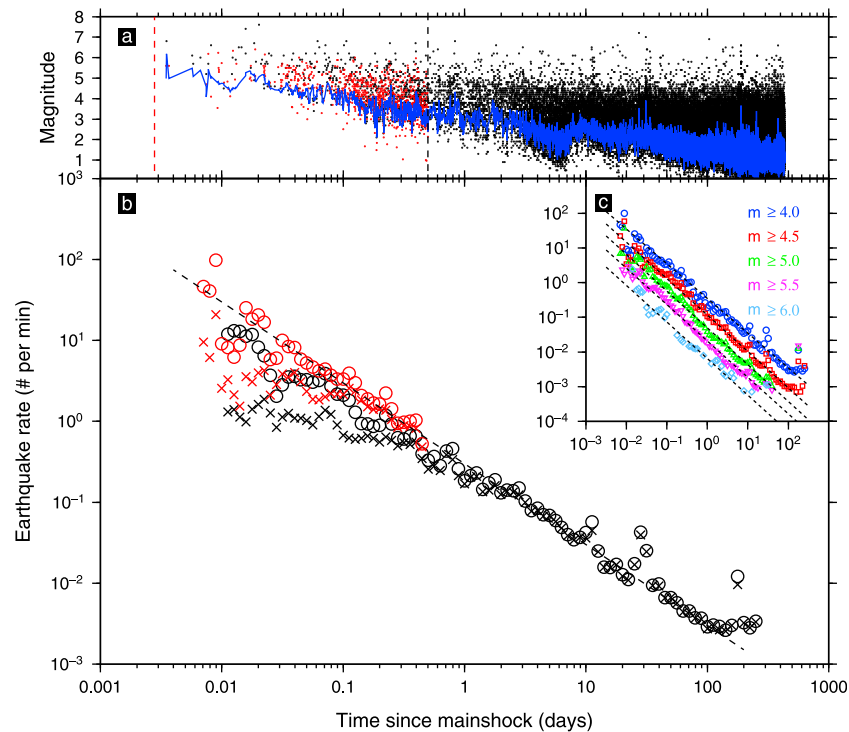
Figure 3. (a) Magnitude against time since mainshock for our newly detected events (red), and events already present in the JMA or Hi-net catalog (black). The red and black dashed lines indicate respectively the 4 minutes and 12 hours time interval after the mainshock. The magnitude of completeness, computed for all the earthquakes, is shown as a blue line (see methods in Text S1). (b) Non-corrected (crosses) and corrected (circles) aftershock ($m \geq 4$) rate against time relative to the mainshock. Aftershock rates including or not the newly detected events are shown in red and black, respectively. A power-law fit with $p = 1.0$ is shown as a dashed line. (c) Corrected earthquake rate including newly detected events computed for different values of magnitude thresholds. Axes are the same as in Figure 3b. Fits of the aftershock decay rates for all magnitude thresholds are displayed as dashed lines and are consistent, within uncertainties, with $p = 1.0$.

[12] We also investigate if there is any space evolution of the aftershock sequence in our newly formed dataset, that includes JMA events in the first 8 days following the mainshock. We remove crustal events and outer rise events from the dataset as they are not directly related to processes on the subduction interface (see discussion in Text S1). This selection is achieved by keeping earthquakes in the boundaries shown in Figure 1 and with a depth greater than 25 km. Although no clear migration is visible, expansion of the aftershock area can be observed along the strike of the subduction plane, particularly in the southward direction (Figure 4). We check that the aftershock expansion is not due to the increase of the number of events at later times (see discussion in Text S1) and look for along dip spreading of events but do not find a pronounced expansion of the aftershock area with depth (Figure S4).

5. Discussion

[13] Our study resolves a continuous decay of the aftershock rate over the whole investigated time-interval with a power-law exponent indistinguishable from $p = 1.0$. At the earliest time, we do not evidence any clear flattening of the earthquake rate limiting us to infer a c-value of the modified Omori law [*Utsu et al.*, 1995] for the aftershock sequence. Our results, however, constrain this value to be less than ~10 minutes, close to the mainshock rupture duration. This

result is similar to those obtained for other aftershock sequences in Japan, where the p-value of the aftershock rate decay is found to be close to 1.0 and the c-value is inferred to be very small [*Enescu et al.*, 2009].

[14] Several interpretations can be advanced to explain the expansion of the aftershock area. It could be argued that static stress transfers from cascading aftershocks might be the motor of this expansion [e.g., *Marsan and Lengliné*, 2010]. Afterslip, developing over the fault plane, might also be responsible for it. Resolving among these two different models is challenging. It is also readily possible that the actual aftershock sequence results from a combination of these two end-member models, i.e., the earthquake stress transfer triggers both seismicity and slow slip, progressively extending the aftershock area.

[15] Several indications suggest a role of the afterslip following the Tohoku mainshock in the observed development of the aftershock sequence. First the location of the aftershocks is focused to the deeper part of the subduction interface, in a region where afterslip is favored because of the frictional condition of the interface compatible with aseismic deformations [*Evans and Meade*, 2012]. Postseismic slip was indeed observed following the mainshock, on the deeper extension of the subduction plane relative to the coseismic slip area [e.g., *Ozawa et al.*, 2011] (see also discussion in Text S1). Then, focal mechanisms of the down dip aftershocks indicate thrust faulting events compatible
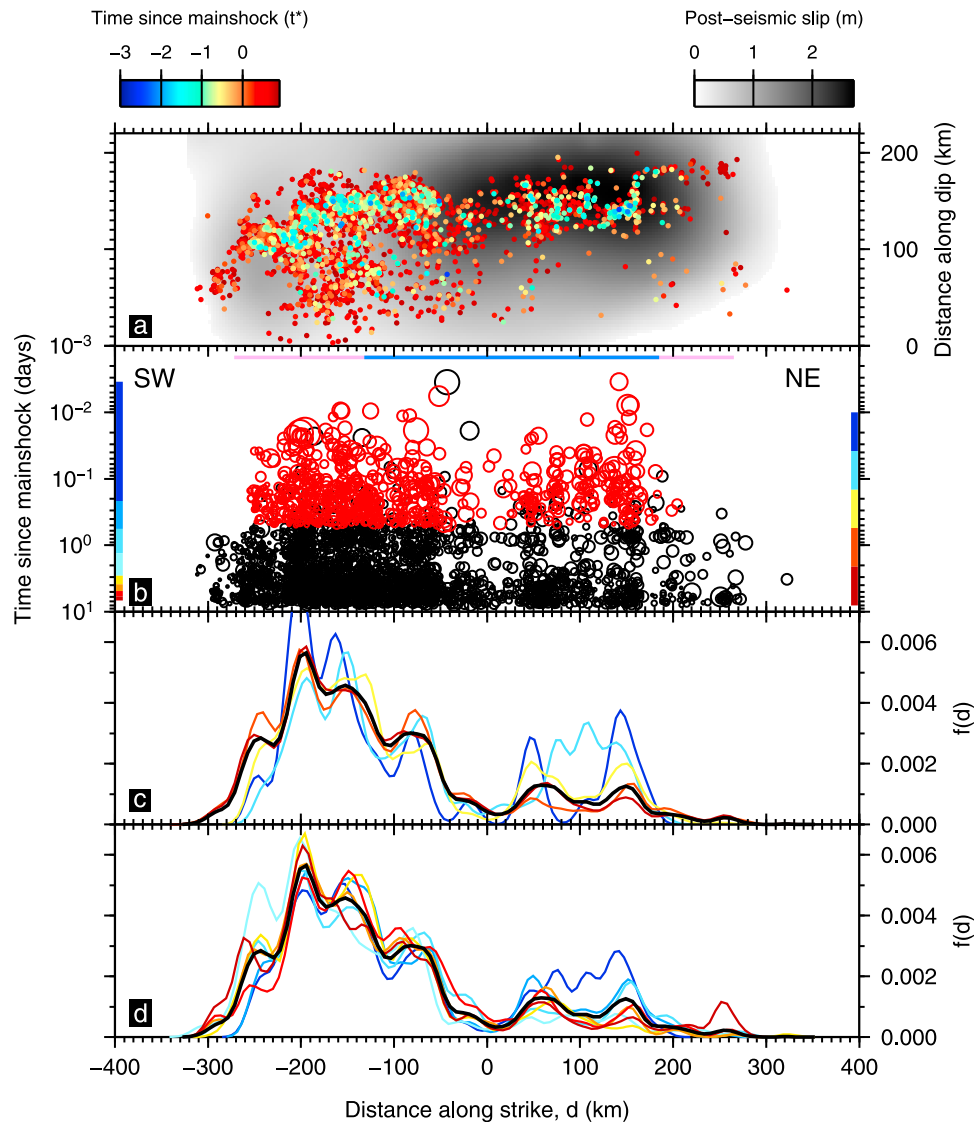
Figure 4. (a) Aftershocks as a function of the along strike distance and the along dip distance (color circles). The color refers to the event occurrence times, $t_* = \log_{10}(t/t_0)$, with t the time since mainshock and $t_0 = 1$ day. Post-seismic slip model of Geospatial Information Authority of Japan (http://www.gsi.go.jp/cais/topic110520-index.html) is shown in grey. (b) Along-strike distance of aftershocks as a function of time since mainshock. Red symbols are events from the Hi-net catalog including newly detected events for the first 12 hours. Black symbols are events in the JMA catalog. The blue and pink horizontal lines correspond to the extension of the coseismic and post seismic slip area, respectively (i.e., slip >80% of the inferred maximum slip). The slip extensions are derived from the co-seismic and post-seismic model of Geospatial Information Authority of Japan (http://www.gsi.go.jp/cais/topic110520-index.html, http://www.gsi.go.jp/cais/topic110314-index.html), respectively. The color bars indicate equally spaced log-time intervals (right) and time intervals containing an equal number (450) of events (left), which were used to draw the probability density distribution of events, $f(d)$, in Figures 4c and 4d. (c) $f(d)$ for equal log-time intervals. (d) $f(d)$ for equal number of event intervals. The thick black line in Figures 4c and 4d refer to the along strike distribution for all events in the sequence. Note the expansion of the pdfs, in particular to the south-west. Quantitative details are presented in the Supplementary Discussion.

with the subduction plane geometry [e.g., *Hirose et al.*, 2011]. It suggests that these earthquakes occurred on the same interface as the post-seismic slip. The extension of this post-seismic slip to the south relative to the coseismic slip area [*Ozawa et al.*, 2011], is also in agreement with the portion of the fault plane where we resolved the aftershock expansion (Figure 4). This zone is also estimated to have a low seismic coupling [*Loveless and Meade*, 2011], compatible with a creeping area including asperities. A better

comparison would require models of post-seismic slip at different time intervals from the mainshock in order to track any progression of the afterslip front in relation to the expansion of the seismicity.

[16] We note that the overall expansion of the aftershock area might also result from a set of localized expanding patches (Figures 4 and S5). The centers of these diffusing patches being not necessarily linked to the location of the biggest aftershocks of the sequence (Figures S4 and S5)

suggest that the observed expansions might be driven by some heterogeneous, developing, post-seismic stress field as also hypothesized by *Kosuga and Watanabe* [2011]. Some of these local afterslip zones may also occur at shallow depth as imaged by repeating aftershocks [*Kato and Igarashi*, 2012].

6. Conclusion

[17] We used a template waveform approach to detect missed earthquakes at early times following the 2011, M_w9.0 Tohoku mainshock. Our results highlight a global expansion of the down dip aftershock area along the strike of the subduction plane to the south and locally around some localized patches of high activity and a continuous decay of the aftershock rate with time. We interpret our observations as the result of a heterogeneous post seismic stress field driving the evolution of the aftershock sequence.

References

Bouchon, M., H. Karabulut, M. Aktar, S. Özalaybey, J. Schmittbuhl, and M.-P. Bouin (2011), Extended nucleation of the 1999 M_w 7.6 Izmit earthquake, *Science*, *331*, 877–880, doi:10.1126/science.1197341.

Enescu, B., J. Mori, M. Miyazawa, and Y. Kano (2009), Omori-Utsu law c-values associated with recent moderate earthquakes in Japan, *Bull. Seismol. Soc. Am.*, *99*, 884–891, doi:10.1785/0120080211.

Evans, E. L. and B. J. Meade (2012), Geodetic imaging of coseismic slip and postseismic afterslip: Sparsity promoting methods applied to the great Tohoku earthquake, *Geophys. Res. Lett.*, *39*, L11314, doi:10.1029/2012GL051990.

Helmstetter, A., and B. E. Shaw (2009), Afterslip and aftershocks in the rate-and-state friction law, *J. Geophys. Res.*, *114*, B01308, doi:10.1029/2007JB005077.

Hirose, F., K. Miyaoka, N. Hayashimoto, T. Yamzaki, and M. Nakamura (2011), Outline of the 2011 off the Pacific coast of Tohoku earthquake (Mw 9.0)—Seismicity: Foreshocks, mainshock, aftershocks, and induced activity, *Earth Planets Space*, *63*(7), 513–518, doi:10.5047/eps.2011.05.019.

Kato, A., K. Obara, T. Igarashi, H. Tsuruoka, S. Nakagawa, and N. Hirata (2012), Propagation of Slow Slip Leading Up to the 2011 Mw 9.0 Tohoku-Oki Earthquake, *Science*, *335*, 705–708, doi:10.1126/science.1215141.

Kato, A. and T. Igarashi (2012), Regional extent of the large coseismic slip zone of the 2011 Mw 9.0 Tohoku-Oki earthquake delineated by on-fault aftershocks, *Geophys. Res. Lett.*, *39*, L15301, doi:10.1029/2012GL052220.

Kilb, D., V. G. Martynov, and F. L. Vernon (2007), Aftershock detection thresholds as a function of time: Results from the ANZA Seismic Network following the 31 October 2001 ML 5.1 Anza, California, earthquake, *Bull. Seismol. Soc. Am.*, *97*, 780–792, doi:10.1785/0120060116.

Kiser, E., and M. Ishii (2012), The March 11, 2011 Tohoku-oki earthquake and cascading failure of the plate interface, *Geophys. Res. Lett.*, *39*, L00G25, doi:10.1029/2012GL051170.

Kosuga, M., and K. Watanabe (2011), Seismic activity around the northern neighbor of the 2011 off the Pacific coast of Tohoku Earthquake with emphasis on a potentially large aftershock in the area, *Earth Planets Space*, *63*(7), 719–723, doi:10.5047/eps.2011.06.006.

Lengliné, O., and D. Marsan (2009), Inferring the coseismic and postseismic stress changes caused by the 2004 M_w = 6 Parkfield earthquake from variations of recurrence times of microearthquakes, *J. Geophys. Res.*, *114*, B10303, doi:10.1029/2008JB006118.

Loveless, J. P., and B. J. Meade (2011), Spatial correlation of interseismic coupling and coseismic rupture extent of the 2011 M_W = 9.0 Tohoku-oki earthquake, *Geophys. Res. Lett.*, *38*, L17306, doi:10.1029/2011GL048561.

Marsan, D., and B. Enescu (2012), Modeling the foreshock sequence prior to the 2011, M_w9.0 Tohoku, Japan, earthquake, *J. Geophys. Res.*, *117*, B06316, doi:10.1029/2011JB009039.

Marsan, D., and O. Lengliné (2010), A new estimation of the decay of aftershock density with distance to the mainshock, *J. Geophys. Res.*, *115*, B09302, doi:10.1029/2009JB007119.

Meng, X., X. Yu, Z. Peng, and B. Hong (2012), Detecting earthquakes around Salton Sea following the 2010 Mw7.2 El Mayor-Cucapah earthquake using GPU parallel computing, *Procedia Comput. Sci.*, *9*, 937–946, doi:10.1016/j.procs.2012.04.100.

Ozawa, S., T. Nishimura, H. Suito, T. Kobayashi, M. Tobita, and T. Imakiire (2011), Coseismic and postseismic slip of the 2011 magnitude-9 Tohoku-Oki earthquake, *Nature*, *475*, 373–376, do:10.1038/nature10227.

Peng, Z., and P. Zhao (2009), Migration of early aftershocks following the 2004 Parkfield earthquake, *Nat. Geosci.*, *2*, 877–881, doi:10.1038/ngeo697.

Peng, Z., J. E. Vidale, M. Ishii, and A. Helmstetter (2007), Seismicity rate immediately before and after main shock rupture from high-frequency waveforms in Japan, *J. Geophys. Res.*, *112*, B03306, doi:10.1029/2006JB004386.

Shelly, D. R., G. C. Beroza, and S. Ide (2007), Non-volcanic tremor and low-frequency earthquake swarms, *Nature*, *446*, 305–307, doi:10.1038/nature05666.

Toda, S., R. S. Stein, and J. Lin (2011), Widespread seismicity excitation throughout central Japan following the 2011 M = 9.0 Tohoku earthquake and its interpretation by Coulomb stress transfer, *Geophys. Res. Lett.*, *38*, L00G03, doi:10.1029/2011GL047834.

Utsu, T., Y. Ogata, and R. S. Matsu'ura (1995), The centenary of the Omori formula for a decay law of aftershock activity, *J. Phys. Earth*, *43*(1), 1–33.